Supplement: Pushing the sample-size limit of infrared vibrational nano-spectroscopy: from monolayer towards single molecule sensitivity

Xiaoji G. Xu,[†] Mathias Rang,[‡] Ian M. Craig,[¶] and Markus B. Rashcke[*,†]

Department of Physics, Department of Chemistry, and JILA, University of Colorado, Boulder, Colorado 80309, United States, Forschungsinstitut am Goetheanum, CH-4143 Dornach, Switzerland, and Pacific Northwest National Laboratory, Richland, Washington 99352, United States

E-mail: markus.raschke@colorado.edu

---

[*]To whom correspondence should be addressed

[†]Department of Physics, Department of Chemistry, and JILA, University of Colorado, Boulder, Colorado 80309, United States

[‡]Forschungsinstitut am Goetheanum, CH-4143 Dornach, Switzerland

[¶]Pacific Northwest National Laboratory, Richland, Washington 99352, United States

Here we provide further technical details on the theoretical analysis of the spectral phase and amplitude of the infrared scattering scanning near-field optical microscopy (IR s-SNOM) response. We discuss in particular the validity and limitations of the spectral phase approximation with regards to the vibrational mode assignment and correspondence of spectral phase behavior with vibrational absorption lineshape. We also present experimental control data that show that when the laser is spectrally detuned from the vibrational resonance, the interferogram exhibits no free induction decay (FID). Finally, we present a table detailing the spectral irradiance of our laser and compare it to other state of the art systems.

Spectral phase approximation

The tip-sample interaction in the presence of an optical field can be analyzed in the quasistatic dipole approximation treating the tip as a small polarizable sphere acting as a scattering element in close proximity to the surface.[1,2] This model qualitatively shows that the near-field spectral phase directly reflects the molecular vibrational resonance energy and lineshape to a good approximation up to a certain molecular oscillator strength as derived below. For a more quantitative description, more refined multilayer models for the tip/molecule/substrate system would have to be used.[3]

The polarizability α of the sphere of radius $r \ll \lambda$ representing the tip with dielectric function ε_t is described by $\alpha = 4\pi r^3 (\varepsilon_t - 1)/(\varepsilon_t + 2)$. With the surface dielectric response given by $\beta = (\varepsilon(\omega) - 1)/(\varepsilon(\omega) + 1)$, with $\varepsilon(\omega)$ the dielectric function of the sample, the effective polarizability describing the tip-sample dipole-coupled system is given by:

$$\alpha_{\text{eff}}(\omega) = \alpha \left(1 - \frac{\alpha\beta}{16\pi(r+d)^3} \right)^{-1} \tag{1}$$

with tip sample distance d.

With the complex dielectric function of the sample given by $\varepsilon(\omega) = \varepsilon_1 + i\varepsilon_2$, we can rewrite β as $\beta = (\varepsilon_1 + i\varepsilon_2 - 1)/(\varepsilon_1 + i\varepsilon_2 + 1)$. For typical infrared vibrational resonances the spectral dispersion across the resonance is in fact weak, hence $\varepsilon_2 \ll \varepsilon_1$. β can then be approximated as:

$$\beta \approx \frac{\varepsilon_1 - 1}{\varepsilon_1 + 1} + i\frac{\varepsilon_2}{\varepsilon_1 + 1} \tag{2}$$

Similarly, the inverse of α can be represented in terms of its corresponding real and imaginary parts:

$$\alpha^{-1} = \frac{1}{4\pi r^3}(\alpha_1 + i\alpha_2) \tag{3}$$

α^{-1} is furthermore related to the effective polarizability as

$$\alpha_{\text{eff}} = \left(\alpha^{-1} - \frac{\beta}{16\pi(r+d)^3} \right)^{-1} \tag{4}$$

Combining Equations 2, 3, and 4 we obtain:

$$\alpha_{\text{eff}} = \left(\frac{1}{4\pi r^3}\alpha_1 - \frac{1}{16\pi(r+d)^3}\frac{\varepsilon_1-1}{\varepsilon_1+1} + i\frac{1}{4\pi r^3}\alpha_2 - i\frac{1}{16\pi(r+d)^3}\frac{\varepsilon_2}{\varepsilon_1+1} \right)^{-1} \tag{5}$$

The phase of α_{eff} is defined as $\theta(\alpha_{\text{eff}}) = -\arctan[\text{Im}(\alpha_{\text{eff}})/\text{Re}(\alpha_{\text{eff}})]$. Hence,

$$\theta(\alpha_{\text{eff}}) = -\arctan\left(\frac{\frac{1}{4\pi r^3}\alpha_2 - \frac{1}{16\pi(r+d)^3}\frac{\varepsilon_2}{\varepsilon_1+1}}{\frac{1}{4\pi r^3}\alpha_1 - \frac{1}{16\pi(r+d)^3}\frac{\varepsilon_1-1}{\varepsilon_1+1}} \right) \tag{6}$$

Substituting $z = (r+d)/r$, Equation 6 simplifies to:

$$\theta(\alpha_{\text{eff}}) = -\arctan\left(\frac{\alpha_2 - \frac{1}{4z^3}\frac{\varepsilon_2}{\varepsilon_1+1}}{\alpha_1 - \frac{1}{4z^3}\frac{\varepsilon_1-1}{\varepsilon_1+1}} \right) \tag{7}$$

For small values of the argument of the arctangent (as justified below), we can use a series expression of Equation 7 and separate the leading term into its resonant and non-resonant contribution. Using $\arctan(x) = x - \frac{1}{3}x^3 + \frac{1}{5}x^5 + \cdots$ and noting that the phase between the resonant and non-resonant terms are additive with $\theta(\alpha_{\text{eff}}) = \theta(\alpha_{\text{eff}})_N + \theta(\alpha_{\text{eff}})_R$, we obtain for the non-resonant phase $\theta(\alpha_{\text{eff}})_N$ in leading order:

$$\theta(\alpha_{\text{eff}})_N \approx -\left(\frac{\alpha_2}{\alpha_1 - \frac{1}{4z^3}\frac{\varepsilon_1-1}{\varepsilon_1+1}} \right) \tag{8}$$

Note that $\theta(\alpha_{\text{eff}})_N$ is only weakly dependent on frequency.

The resonant contribution $\theta(\alpha_{\text{eff}})_R$ is given by:

$$\theta(\alpha_{\text{eff}})_R \approx \left(\frac{\frac{1}{4z^3}\frac{1}{\varepsilon_1+1}}{\alpha_1 - \frac{1}{4z^3}\frac{\varepsilon_1-1}{\varepsilon_1+1}} \right)\varepsilon_2 \tag{9}$$

As stipulated above, only the imaginary part of the molecular dielectric function ε_2 has a strong frequency dependence. Replacing ε_2 with $2nk(\omega)$, we then arrive at:

$$\theta(\alpha_{\text{eff}}) = \theta(\alpha_{\text{eff}})_N + \left(\frac{\frac{1}{2z^3}\frac{1}{\varepsilon_1+1}}{\alpha_1 - \frac{1}{4z^3}\frac{\varepsilon_1-1}{\varepsilon_1+1}} \right)nk(\omega) \tag{10}$$

Equation 10 indicates that the variation in spectral phase of the tip sample polarizability, and thus the IR-vib s-SNOM signal near a molecular resonance, is linearly dependent on the molecular absorption spectrum. This allows for a direct mode assignment from the maximum and lineshape of the spectral phase.

The underlying approximation is valid for moderate vibrational transition probabilities and small spectral variations of the refractive index. Those conditions are fulfilled to a good approximation for most molecular oscillators including C=O, O-H, C-H, and the majority of combination modes. Deviations from this approximation are expected for larger molecular oscillator strengths,

strong phonon polaritons, and electronic resonances.

Example calculation

In this section we provide some sample calculations to illustrate the validity of the spectral phase approximation derived above. Returning to Equation 7, it is instructive to inspect the four terms α_1, α_2, $\frac{1}{4z^3}\frac{\varepsilon_2}{\varepsilon_1+1}$, and $\frac{1}{4z^3}\frac{\varepsilon_1-1}{\varepsilon_1+1}$ individually. From Equation 3, we can calculate expressions for α_1 and α_2

$$\alpha_1 = 1 + \frac{3(\varepsilon_{t1}-1)}{(\varepsilon_{t1}-1)^2 + \varepsilon_{t2}}, \qquad \alpha_2 = -\frac{3\varepsilon_{t2}}{(\varepsilon_{t1}-1)^2 + \varepsilon_{t2}} \tag{11}$$

with $\varepsilon_t = \varepsilon_{t1} + i\varepsilon_{t2}$. For typical metals in the infrared, such as the common tip material Pt, α_1 is close to unity, and α_2 is smaller than α_1 by two orders of magnitude, both with weak spectral variation. 1a shows the values of α_1 and α_2 calcualted for Pt in the vicinity of the carbonyl frequency (data for the dielectric function taken from Reference[4]). Figure 1b shows the refractive index and extinction coefficient for a typical carbonyl dielectric function derived from spectroscopic ellipsometry.[5] Finally, the terms $\frac{1}{4z^3}\frac{\varepsilon_2}{\varepsilon_1+1}$ and $\frac{1}{4z^3}\frac{\varepsilon_1-1}{\varepsilon_1+1}$, based on the data shown in (a) and (b), are plotted in Figures 1c–d, for a tip-substrate distance of $d = 0$ ($z = 1$). As the tip is removed from the surface, the shape of the profiles will not change, but will scale as z^{-3}.

The ratio $\alpha_1 : \frac{1}{4z^3}\frac{\varepsilon_1-1}{\varepsilon_1+1} : \frac{1}{4z^3}\frac{\varepsilon_2}{\varepsilon_1+1} : \alpha_2$ is approximately $1 : 0.1 : 0.025 : 0.0025$. Consequently the argument of the arctangent in Equation 6 is dominated by $\frac{1}{4z^3}\frac{\varepsilon_2}{\varepsilon_1+1}$ in the numerator and α_1 in the denominator. The ratio between numerator and denominator is about 1:40, and $\frac{1}{4z^3}\frac{\varepsilon_2}{\varepsilon_1+1}$ is linearly proportional to the imaginary part of the dielectric function of the sample as shown previously, and we thus justify the approximation underlying Equation 9.

Alternatively, Equation 9 can be written as:

$$\theta(\alpha_{\text{eff}}) \approx \frac{2nk(\omega)}{4z^3\alpha_1(\varepsilon_1+1) - \varepsilon_1 - 1} \tag{12}$$

With n, α_1, and ε_1 varying slowly across the resonance (see Figure 1b), $\theta(\alpha_{\text{eff}})$ thus mirrors the vibrational absorption profile through $k(\omega)$.

Limitations of the spectral phase approximation

The approximation of $\arctan(x) \approx x$ is valid for $x \lesssim 0.05$ for typical vibrational resonances with few cm^{-1} precision. In the case discussed above the value is $x \sim 0.025$. Figure 2 shows a numerical simulation of the effect of an increasing resonant vibrational extinction coefficient $k(\omega)$ (Figure 2a) on the spectral phase behavior α_{eff} (Figure 2b). The spectral phase scales approximately linearly with oscillator strength. With increasing oscillator strength a small blue shift of several cm^{-1} is observed as the approximation $\arctan(x) \approx x$ breaks down.
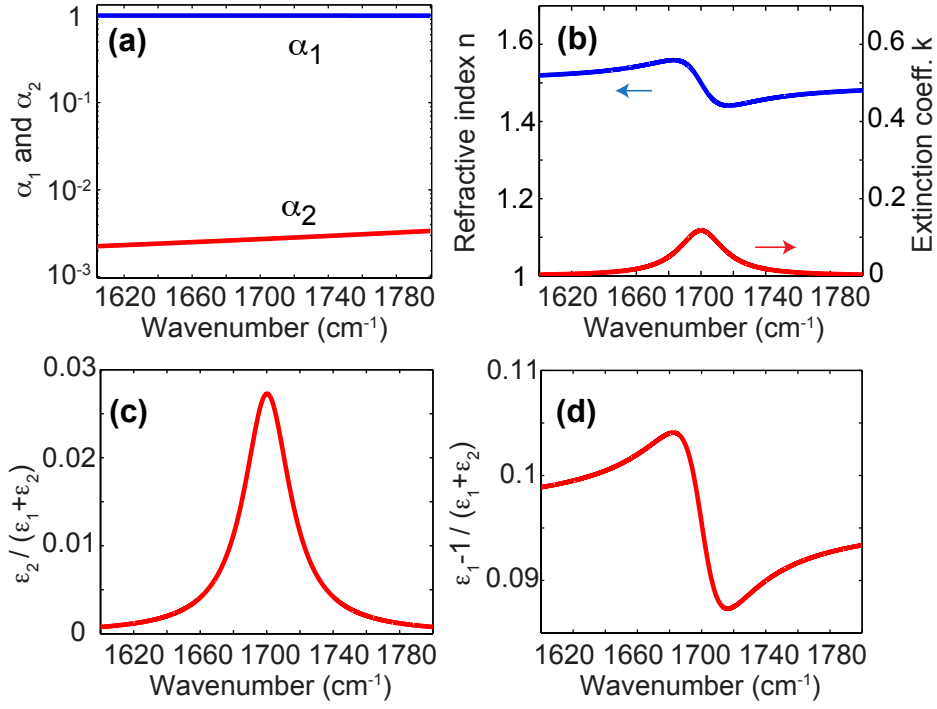
Figure 1: Example calculation of the different terms contributing to Equation 6 for a Pt tip coupling to a model carbonyl mode: a) α_1 (blue) and α_2 (red). Note the vertical log scale. b) Refractive index (blue) and extinction coefficient (red) for typical carbonyl mode.[5] Corresponding terms c) $\frac{1}{4z^3}\frac{\varepsilon_2}{\varepsilon_1+1}$ and d) $\frac{1}{4z^3}\frac{\varepsilon_1-1}{\varepsilon_1+1}$ for $z = (r+d)/r = 1$. Note that the amplitudes in c) and d) scale with distance as z^{-3} with the same profile shape.
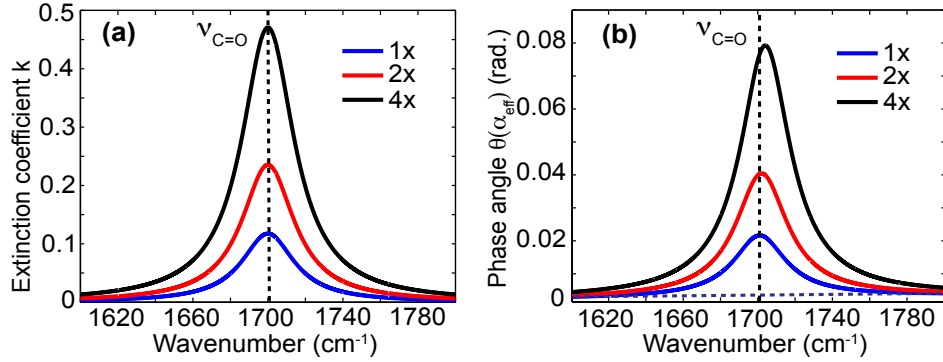
Figure 2: a) Influence of an increase in extinction coefficient $k(\omega)$ for 1, 2 and 4 times a typical C=O oscillator strength on b) the spectral phase behavior α_{eff}. Dashed vertical lines represent the vibrational transition energy. A small blue shift in the spectral phase $\theta(\alpha_{\text{eff}})$ for large extinction coefficient is a result of the deviations from the approximation $\arctan(x) \approx x$. The horizontal line in b) shows the slowly varying baseline due to the small dispersion of the dielectric function of the metallic tip.

Substrate enhancement

Our approximation above is based on the assumption that the dielectric function of the sample is much smaller than the dielectric function of the metallic tip. In our work, in order to increase the sensitivity, we use a metallic substrate to enhance the local electric field. The metal, however, influences the dielectric function of the sample consisting of the molecular film and substrate, which must be accounted for. In order to qualitatively describe the effect we replace the dielectric function of the molecular oscillator of interest with an effective dielectric function of the substrate and molecule. This model provides for an intuitive picture; for a more quantitative description a model describing the scattering from multiple interfaces would need to be used.[3]
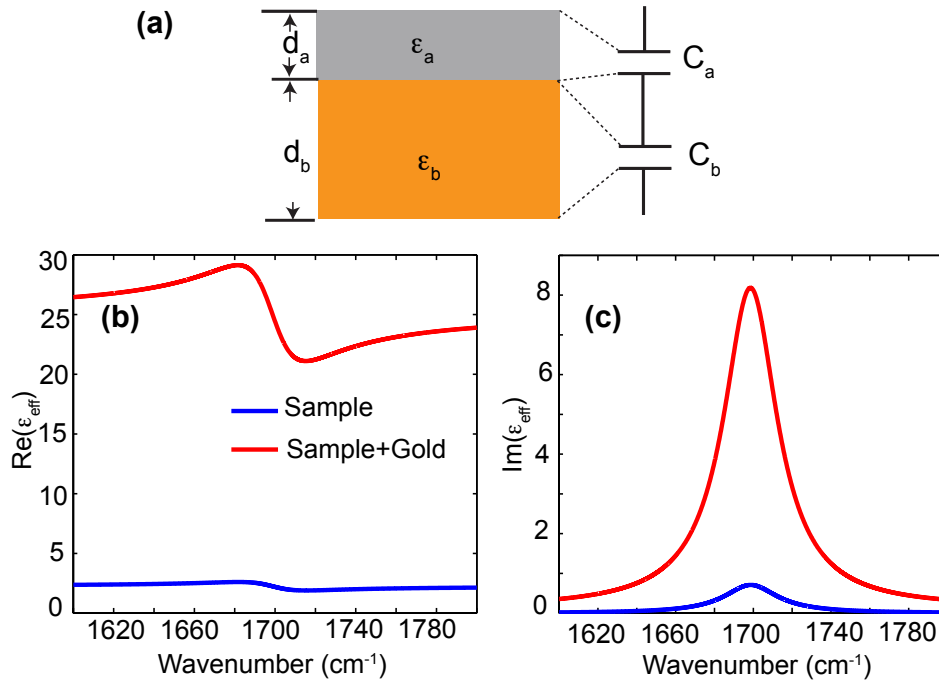
Figure 3: a) Schematic of a sample consisting of molecular film with dielectric function ε_a and thickness ε_a on a gold substrate with dielectric function ε_b and optical penetration depth d_b and its conceptual analogy to two capacitors in series . b) Real and c) Imaginary parts of sample dielectric function (blue) and sample/substrate effective dielectric function (red) for a thickness ratio of $d_a : d_b = 10 : 1$. The presence of a metal substrate enhances the imaginary part of the dielectric function at the vibrational resonant frequency.

In the quasistatic limit, a polarizable material will have excess charge at a boundary, conceptually similar to charged capacitor. With the polarizability of a thin layer on top of a substrate described by bound charges, the system can be treated as two capacitors in series of thickness d_a and d_b, where d_b is more precisely linked to the optical penetration depth (see Figure 3a). With the respective dielectric functions ε_a and ε_b, the capacitance of each layer is $C_a \propto \varepsilon_a/d_a$ and $C_b \propto \varepsilon_b/d_b$.

Using $C_{\text{eff}}^{-1} = C_{\text{a}}^{-1} + C_{\text{b}}^{-1}$, the effective dielectric function is found to be:

$$\varepsilon_{\text{eff}} = \frac{d_{\text{a}} + d_{\text{b}}}{d_{\text{a}}\varepsilon_{\text{a}}^{-1} + d_{\text{b}}\varepsilon_{\text{b}}^{-1}} \tag{13}$$

As an example, for $d_{\text{a}} : d_{\text{b}} = 10 : 1$ Figure 3a–b shows the enhancement of the signal in terms of the resulting $\varepsilon_{\text{eff}} = \varepsilon_{1,\text{eff}} + i\varepsilon_{2,\text{eff}}$. However, this substrate enhancement of the effective dielectric function can lead to deviations from the spectral phase approximation. In the example given, $\frac{1}{4z^3}\frac{\varepsilon_2}{\varepsilon_1+1}$ is no longer much smaller than α_1 (in this specific example the ratio is 0.1). Depending on the degree of substrate enhancement this could influence the interpretation of monolayer or few nanometer thick films. Interestingly, the presence of a far-field background diminishes that effect to some extent. The far-field scattering from, e.g., the tip shaft decreases the spectral phase shift, effectively increases the real part of the tip/sample polarizability, hence increasing the denominator in the arctangent function, thus reducing the spectral phase shift across the resonances.
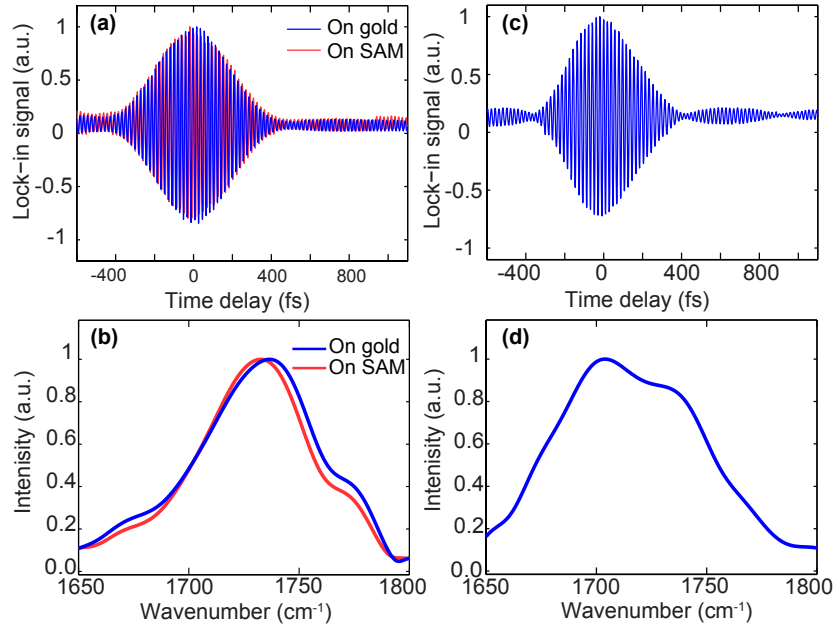
Figure 4: (a) Interferograms with laser detuned from the carbonyl resonance to $1740\,\text{cm}^{-1}$ showing nearly identical shapes when acquired on SAM (red profile) compared to clean gold (blue profile). The corresponding Fourier transformed spectra (b) of interferograms obtained in (a). (c) Interferogram with the laser tuned back to $1700\,\text{cm}^{-1}$ and data taken with a bare gold sample, again with absence of FID behavior.

Reference interferograms with laser detuned

To ensure that the spectral contrast observed experimentally is a resonant effect and not an experimental artifact, interferograms are taken on the same SAM, but with the laser detuned from the resonance frequency by $40\,\text{cm}^{-1}$ (Figure 4a, red), and on bare gold substrates with the laser tuned

to 1700 cm^{-1} (blue). Figure 4b shows the associated Fourier transform. Both figures show that off resonance, the MHDA is invisible and has no effect on the near-field response. Similarly, Figure 4c shows the interferogram on bare gold with the laser tuned back to 1700 cm^{-1} and shows no FID behavior (Fourier transform, Figure 4d).

Spectral contrast of two spatially separate locations

Although chemically largely homogeneous, sample nano-scale spatial variation of the spectral response is observed (see Figure 5). The 16-mercaptohexadecanoic acid (MHDA) nanocrystals reduce the enhancement via the metal substrate and therefore slightly reduce the spectral contrast in both amplitude and spectral phase. The spectral similarity indicate dimer formation both for the SAMs as well as for the nanocrystals.
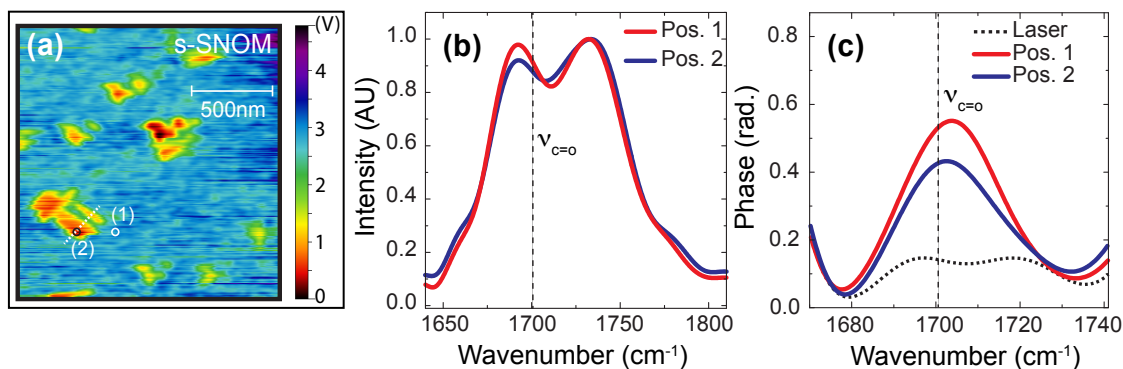
Figure 5: a) *s*-SNOM optical image of MHDA SAM and MHDA nanocrystals at the two measurement points marked in the image as (1) and (2). b) The Fourier transformed spectra of the interferograms obtained from two spatial locations of the flat SAM at (1) (red) and nanocrystals at (2) (blue). c) From the Fourier transform, corresponding spectral phase of the two sample positions compared with the laser reference spectral phase scattered from the withdrawn tip.

Phase unfolding raw lock-in data

Our data is collected using a photoconductive detector which responds to intensity and therefore always returns a positive signal, measured on our lock-in amplifier. However, when the phase difference between the measurement arm and the reference arm crosses zero, the phase of the lock-in signal goes through a π phase shift. When collecting data, we record both the intensity and the phase at each delay point. Afterwards, we use MATLAB to reverse the sign of the intensity everywhere the lock-in phase flips to unfold the interferrogram and recover the data as presented. The Fourier transforms, spectral phase analysis, and short-time Fourier transform spectrograms are all done using the fft function of MATLAB.

Spectral irradiance of relevant mid infrared laser sources

The characteristics of our laser source and other relevant mid-infrared light sources for s-SNOM infrared nanoscopy are listed in the table below. For the coherent sources, we assume a focused spot size diameter of 20 μm. The 1:1 beam splitter in the interferometer setup is considered in the estimation of irradiance at the focus.

For the thermal source, we assume a 50 W glowbar of active area 10mm^2 with 90% IR emission efficiency and a blackbody emission bandwidth of 4000 cm^{-1}. The emission radiates into a 4π solid angle and is collected with a 0.25 NA IR lens with no other losses. Because the irradiance at the focus cannot exceed the irradiance at the source for spatially incoherent light, this is the upper limit for irradiance in a near-field experiment with a thermal source.

Another type of thermal near-field technique using a heated tip[6] is not listed here for comparison because of the considerable differences in instrumentation.

Table 1: Comparison of current IR light sources for *s*-SNOM

	This work	Amarie et. al.[7]	QCL	Thermal source[8]
Power	1 mW	25 μW	$\sim$100 mW	$\sim$45W
Bandwidth	80 cm^{-1}	200 cm^{-1}	1 cm^{-1}	4000 cm^{-1}
Est. Focal Area	$3 \times 10^{-6}\ \text{cm}^2$	$3 \times 10^{-6}\ \text{cm}^2$	$3 \times 10^{-6}\ \text{cm}^2$	0.1 cm^2
Spatial Coherence?	Yes	Yes	Yes	No
Multiplex?	Yes	Yes	No	Yes
Est. Spectral Irradiance at Focus (W/cm^2/cm^{-1})	2	2.1×10^{-2}	1.7×10^4	9×10^{-4}

References

(1) Keilmann, F.; Hillenbrand, R. Near-Field Microscopy By Elastic Light Scattering From a Tip. *Phil. Trans. R. Soc. A* **2004**, *362*, 787.

(2) Raschke, M. B.; Lienau, C. Apertureless Near-Field Optical Microscopy: Tip-Sample Coupling in Elastic Light Scattering. *Appl. Phys. Lett.* **2003**, *83*, 5089–5091.

(3) Aizpurua, J.; Taubner, T.; de Abajo, F. J. G.; Brehm, M.; Hillenbrand, R. Substrate-Enhanced Infrared Near-Field Spectroscopy. *Opt. Express* **2008**, *16*, 1529.

(4) Palik, E. D., Ed. *Handbook of Optical Constants of Solids*; Academic Press: San Diego, 1985.

(5) Angelova, P.; Hinrichs, K.; Esser, N.; Kostova, K.; Tsankov, D. Self-Assembly of Terminally Aryl-Substituted Long-Chain Alkanethiols on Silver. *Vib. Spectrosc.* **2007**, *45*, 55.

(6) Jones, A. C.; Raschke, M. B. Thermal Infrared Near-Field Spectroscopy. *Nano Lett.* **2012**, *12*, 1475–1481.

(7) Amarie, S.; Zaslansky, P.; Kajihara, Y.; Griesshaber, E.; Schmahl, W. W.; Keilmann, F. Nano-FTIR Chemical Mapping of Minerals in Biological Materials. *Beilstein J. Nanotechnol.* **2012**, *3*, 312–323.

(8) Huth, F.; Schnell, M.; Wittborn, J.; Ocelic, N.; Hillenbrand, R. Infrared-Spectroscopic Nanoimaging with a Thermal Source. *Nat. Mater.* **2011**, *10*, 352–356.